Journal of Applied Physics

RESEARCH ARTICLE | DECEMBER 17 2021

Understanding copper diffusion in $CuInSe_2$ with first-principles based atomistic and continuum models

David E. Sommer ; Scott T. Dunham

Check for updates

Journal of Applied Physics 130, 235701 (2021)
https://doi.org/10.1063/5.0075265
CHORUS

View Online
Export Citation
CrossMark

Articles You May Be Interested In

A photoluminescence study of excitonic grade $CuInSe_2$ single crystals irradiated with 6 MeV electrons

Journal of Applied Physics (October 2015)

Defect segregation at grain boundary and its impact on photovoltaic performance of $CuInSe_2$

Appl. Phys. Lett. (May 2013)

Novel approach to $CuInSe_2$-based thin-film photovoltaic cells

Appl. Phys. Lett. (September 1992)

30 August 2023 13:45:23

AIP Publishing

Journal of Applied Physics ARTICLE scitation.org/journal/jap

Understanding copper diffusion in $CuInSe_2$ with first-principles based atomistic and continuum models

Cite as: J. Appl. Phys. **130**, 235701 (2021); doi: 10.1063/5.0075265
Submitted: 14 October 2021 · Accepted: 28 November 2021 ·
Published Online: 17 December 2021

View Online Export Citation CrossMark

David E. Sommer[1,a] and Scott T. Dunham[2]

AFFILIATIONS

[1]Department of Physics, University of Washington, Seattle, Washington 98195, USA
[2]Department of Electrical Engineering, University of Washington, Seattle, Washington 98195, USA

[a]**Author to whom correspondence should be addressed:** dsommer55@gmail.com

ABSTRACT

We investigate the diffusion of copper in $CuInSe_2$ using thermodynamic and kinetic models based on density functional theory calculations, attempting to reconcile large differences in reported experimental diffusivities. We find that observations of rapid chemical diffusion can be explained by large thermodynamic factors, which we calculate using a compositionally constrained model of intrinsic point defect formation. We further characterize how copper diffusion coefficients depend on material synthesis conditions and exhibit their variation across the $CuInSe_2$ secondary phase diagram. In doing so, we identify stable off-stoichiometries that are dominated by either vacancy- or interstitial-mediated diffusion mechanisms. These results are employed in the development of a continuum reaction–diffusion model, which we use to simulate experimental depth profiles.

Published under an exclusive license by AIP Publishing. https://doi.org/10.1063/5.0075265

30 August 2023 13:45:23

I. INTRODUCTION

The chalcopyrite semiconductor $CuInSe_2$ (CIS) is widely recognized as a promising absorber layer for low-cost, high-efficiency thin-film photovoltaics (PVs) due to its intrinsic tolerance to the presence of crystalline disorder.[1–3] Indeed, much effort has been applied toward characterizing the atomistic defect properties of the material and the development of optimal protocols for device fabrication.[4–7] For example, it is well-appreciated that CIS is heavily compensated by the formation of a diverse range of point defects and their complexes,[7–12] leading to stable material compositions, which can deviate substantially from ideal stoichiometry.[13,14] This flexibility is often advantageous, as it allows the electronic properties of the material to be effectively controlled by the material synthesis conditions and post-synthetic defect engineering.

The Cu composition, in particular, is observed to play a crucial role in dictating PV device performance, where it has been found that Cu-poor, Se-rich materials lead to high-efficiency *p*-type absorbers.[14] From an atomistic perspective, Cu-deficient stoichiometries disfavor the formation of Cu_{In} antisites, which can act as deep recombination centers, while promoting the formation of shallow Cu vacancies. The high mobility of Cu vacancies can, in turn, facilitate the diffusion of beneficial alkaline dopants as well as the stabilization of various defect complexes,[15] and understanding Cu diffusivity in $Cu(In,Ga)Se_2$ could help resolve the underlying mechanism for the recently observed correlation between Na doping and In/Ga interdiffusion.[15,16] Indeed, Cu itself is a particularly mobile species, and its migration can locally change the self-doping in a CIS absorber layer. This is thought to be essential for *p–n* junction formation at the CdS–CIS interface and, thus, on the subsequent quality of the PV device.[14,17–19]

Previous experimental work has found that Cu diffusion can depend significantly on material composition, with reported[17,20–25] values of the Cu diffusivity varying over several orders of magnitude (10^{-12}–10^{-8} cm^2/s) at elevated temperature (500–700 K). Recent first-principles calculations[26,27] support the conclusion[20–22] that Cu vacancies play a fundamental role in mediating diffusion, while also highlighting the potentially significant contribution of Cu interstitials. The role of material composition in Cu-vacancy-mediated diffusion was further explored in Ref. 28, where a combination of thermodynamic calculations, and kinetic lattice Monte Carlo (KLMC) simulations parameterized by first-principles calculations

Published under an exclusive license by AIP Publishing

showed that large variations in the Cu-vacancy concentration could account for some of the differences in the experimental diffusivities.

In this work, we extend that analysis,[28] following Ref. 27, by including the contributions of Cu interstitial diffusion and more realistic constraints on the material synthesis conditions. In particular, we model the total Cu diffusivity across the full thermodynamic stability range of CIS and numerically quantify the difference between so-called *tracer* and *chemical* diffusion coefficients. In doing so, we disentangle two effects that can contribute to larger measured values of Cu diffusivity. First, in the absence of significant Cu composition gradients and in the limit where the concentration of tracked particles, such as radioactive tracers, is small, the measured Cu diffusivity is largely controlled by the composition. This dictates the relative contributions of vacancy and interstitial mechanisms, and for Cu-rich compositions, we find that a sufficient number of rapidly diffusing interstitials dominates the total diffusivity. Conversely, when significant Cu concentration gradients exist, for instance, near the interface between CIS phases of disparate compositions or between CIS and some secondary phase, one enters the regime of chemical diffusion. In this case, we find that the inclusion of an extra thermodynamic factor can account for observed diffusivities 2–3 orders of magnitude larger than tracer self-diffusion. This thermodynamic factor arises from the gradient in chemical potential due to the composition gradient that gives an effective drift term that goes beyond standard entropy-driven diffusion. To validate the consistency of this picture, which is fundamentally based on a linear response approximation, we build a minimal continuum model that we then use to simulate a typical experimental Cu diffusion measurement. Strong agreement with available experimental data[22,29] supports the fundamental role played by local variations in Cu composition in interpreting diffusion measurements.

II. METHODS AND MODEL SELECTION

The rearrangement of native cations in CIS depends on the availability of atomistic pathways mediating their diffusion. Since the local hopping of atoms in semiconducting crystals tends to be thermally activated, a given hop will depend on a migration energy barrier separating the initial and final configurations.[30] Moreover, the likelihood that such a transition is thermodynamically accessible in the first place is determined by the probability to find the local initial configuration in the system. For defect-mediated diffusion processes, this probability is given by the fractional concentrations of the participating defects and their local binding energies. The equilibrium concentration of intrinsic defects in complex semiconductor compounds with semi-ionic character such as CIS will generally depend on the underlying composition of the material.[31] Thus, the characterization of diffusion mechanisms in CIS requires a model for the underlying defect concentrations as a function of composition at relevant temperatures.

The contribution of a particular diffusion mechanism mediated by defect d in net charge state q to the total diffusivity, $D^*_{\mathrm{tot}} = \sum_{d,q} D^*_{d,q}$, of a given species, α, can be approximated using the typical Langmuir–Arrhenius form for the tracer diffusion coefficient,

$$D^*_{d,q} = gf\lambda^2 p_{d,q} \nu e^{-\Delta E^{(m)}_{d,q}/k_{\mathrm{B}}T}, \tag{1}$$

where λ is the hopping distance, $\Delta E^{(m)}_{d,q}$ is the migration energy barrier, f is a correlation factor dependent on the mechanism and the underlying crystalline lattice, and $g = z/2d$ is a geometric factor determined by the nearest-neighbor coordination number z and the spatial dimension d of the diffusion process. The attempt frequency ν characterizes the equilibrium thermal motion around the initial configuration projected onto the reaction coordinates. While typically on the order of the Debye frequency of the lattice, it can be approximated, at the level of quasi-harmonic transition state theory,[32,33] by the normal vibrational modes around the ground state, $\nu^{(G)}_j$, and saddle point, $\nu^{(S)}_j$, configurations,

$$\nu = \frac{\prod_j^{3N} \nu_j^{(G)}}{\prod_j^{3N-1} \nu_j^{(S)}}. \tag{2}$$

Migration energy barriers were calculated using the climbing-image nudged elastic band (CINEB) method[34] and density functional theory (DFT),[35] while normal vibrational modes were calculated using density functional perturbation theory (DFPT). Additional details on the first-principles calculations used to derive model parameters are given in the Appendix.

Near equilibrium, the probability, $p_{d,q}$, that the defects mediating diffusion in net charge state q are locally available depends on their equilibrium fractional concentrations, $x_{d,q}$. These defect concentrations are given by $x_{d,q}/(1 - x_{d,q}) = \theta_{d,q} e^{-\Delta E^{(f)}_{d,q}/k_{\mathrm{B}}T}$, where the formation energy,

$$\Delta E^{(f)}_{d,q} = E_{d,q} - E_{\mathrm{bulk}} + \sum_\alpha m^\alpha_d \mu_\alpha + q(E_{\mathrm{VBM}} + E_{\mathrm{Fermi}}) + E_{\mathrm{corr}}, \tag{3}$$

can be derived from DFT using the supercell method,[36] and $\theta_{d,q}$ is a degeneracy factor accounting for entropic contributions to the defect free energy. Typically, we find that $x_{d,q} \ll 1$, while highly defective stoichiometries lead to small corrections to this dilute approximation on the order of a couple percent. Crucially, the formation energies depend on a set of chemical potentials, $\mu_\alpha = \mu^0_\alpha + \Delta\mu_\alpha$, whose deviations $\Delta\mu_\alpha$ with respect to a standard reference μ^0_α characterize the synthesis conditions of the material. While these chemical potentials can be constrained by requiring stability against secondary phase formation, their absolute values are nonetheless difficult to choose without extensive experimental data. However, net atomic fractions k_α are readily measurable, and given a set of expected defects in the system, one can calculate deviations from perfect stoichiometry,[37] k^p_α, by

$$k_\alpha = \frac{k^p_\alpha - \sum_{d,q} x_{d,q} m^\alpha_d}{1 - \sum_{d,q} x_{d,q} \sigma_d}, \tag{4}$$

where $\sigma_d = \sum_\alpha m^\alpha_d$ and m^α_d is the number of atoms of species α removed in the formation of a single defect, d. Given a set of atomic fractions and standard reference chemical potentials, one can self-consistently obtain defect concentrations, total chemical potentials,

30 August 2023 13:45:23

Published under an exclusive license by AIP Publishing

and the equilibrium Fermi level by solving the inverse problem[37] defined by (4). By imposing compositional constraints, this method, which we subsequently refer to as compositionally constrained thermodynamics (CCT), amounts to modeling the defect thermodynamics in the canonical ensemble. Of course, there is a one-to-one correspondence between atomic fractions k_α and chemical potentials μ_α, and in determining defect concentrations, one is free to set a combination that spans the chemical space of the material of interest. This results in a mixed canonical/grand canonical treatment of the defect thermodynamics. The CCT models used in this work include an extensive set of intrinsic defects,[9,31] namely, all cation and anion vacancies (V_{Cu}, V_{In}, V_{Se}) and interstitials (Cu_i, In_i, Se_i), cation antisites (In_{Cu}, Cu_{In}), and typically prevalent defect complexes ($V_{Cu}-In_{Cu}$, $2V_{Cu}-In_{Cu}$, $V_{Cu}-V_{Se}$).

The region of thermodynamically (meta)stable CIS spans a broad range of Cu compositions in the experimental In_2Se_3–Cu_2Se pseudobinary phase diagram,[38,39] extending largely toward the Cu-poor side of ideal stoichiometry and less so into the Cu-rich side, $0.65 \lesssim k_{Cu}/k_{In} \lesssim 1.05$. Furthermore, excess Se supplied during material growth leads to *p*-type CIS, characterized by a nominal valence ratio $2k_{Se}/(k_{Cu}+3k_{In}) > 1.0$. Figure 1 exhibits this relationship, predicted by CCT calculations at 700 K, relative to the secondary phase diagram predicted by DFT. It is worth noting that the predicted phase boundaries are based on zero-temperature ground state formation enthalpies, and therefore, variations on the order of k_BT should be expected at finite temperature. This accounts for the degree to which the displayed composition maps extend beyond the ideal, 0 K CIS region.

Let us discuss some salient features of Fig. 1, which will be relevant to our analysis of Cu diffusion in Sec. III. As expected, the largest changes in composition occur near the phase boundaries, signaled by large fluctuations in the relevant particle numbers $\langle(\delta N_\alpha)^2\rangle = k_BT\partial\langle N_\alpha\rangle/\partial\mu_\alpha$. For example, the boundary shared with the Cu-depleted phase $CuIn_5Se_8$ features steep gradients in the cation, k_{Cu}/k_{In}, and anion–cation $k_{Se}/(k_{Cu}+k_{In})$ ratios. This is accompanied by the formation of Cu vacancies, In_{Cu} antisites, and their stabilized complexes $nV_{Cu}-In_{Cu}$ ($n=1,2$). Indeed, upon decreasing Cu composition, CIS is found to become unstable relative to the formation of mixed ordered defect compound (ODC) phases,[39] and this is often attributed to the aggregation of large

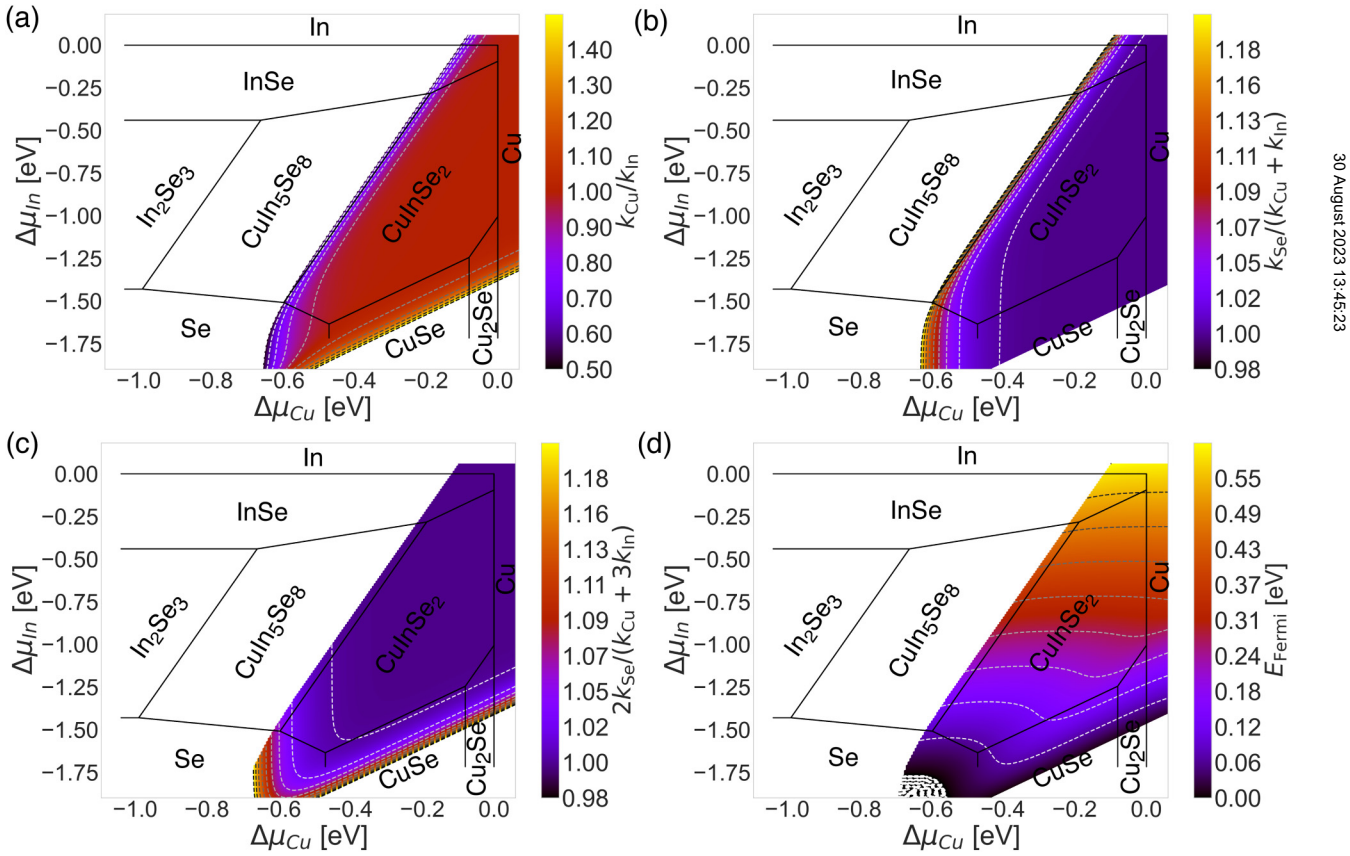

FIG. 1. Predicted variations of the CIS composition (a)–(c) and a self-consistent Fermi level (d) at 700 K mapped to the secondary phase diagram. Shown are (a) the [Cu]/[In] cation ratio, (b) the [Se]/([Cu]+[In]) anion–cation ratio, and (c) the nominal valence ratio 2[Se]/([Cu]+3[In]). Sparse isocurves (white, dashed curves) are included to highlight the nonlinearity in the mapping between chemical potential and composition space.

30 August 2023 13:45:23

Published under an exclusive license by AIP Publishing

numbers of $n\mathrm{V_{Cu}}$–$\mathrm{In_{Cu}}$ complexes.[40,41] Near the pure Se and $\mathrm{Cu}_x\mathrm{Se}$ boundaries, we find large changes in the nominal valence ratio and the cation ratio. Variations in the self-consistent Fermi level are also shown and found to agree with the model results in Ref. 42 and the experimental study in Ref. 43, where larger Se chemical potential/partial pressure led to stronger *p*-type doping. Indeed, approaching the Se phase boundary requires decreasing the Cu chemical potential, leading to a proliferation of Cu vacancies, which act as shallow acceptors. For fixed Se chemical potential, we also find that increasing the [Cu]/[In] ratio decreases the Fermi level[14] due primarily to decreases in the concentration of $\mathrm{In_{Cu}}$, which acts as a shallow donor, and increasing $\mathrm{Cu_{In}}$, which features an acceptor level close to the valence band.[7] While approaching these Cu-rich secondary phases, not only does the In sublattice become increasingly replaced by Cu, but open interstitial sites become occupied by Cu as well. This Cu saturation eventually destabilizes the chalcopyrite CIS lattice, allowing for phase separation of $\mathrm{Cu}_x\mathrm{Se}$. Indeed, the synthesis of Cu-rich CIS often requires the removal of surface $\mathrm{Cu_2Se}$ by wet chemical etching.[44] Moreover, the formation of Cu interstitials in Cu-rich CIS is consistent with recent nanostructure measurements using atom probe tomography, which showed evidence for the existence of metastable Cu supersaturation.[44]

In the absence of concentration gradients, the diffusive motion of individual tracer particles is well-described by the tracer diffusion coefficients (1). Formally speaking, these can be derived on the basis of a Green–Kubo formula,

$$D_\alpha^* = \frac{1}{N_\alpha d}\sum_{i=1}^{N_\alpha}\int_0^\infty dt\langle \mathbf{v}_i(t)\cdot\mathbf{v}_i(0)\rangle, \tag{5}$$

where $\langle\cdot\rangle$ denotes an equilibrium ensemble average, and the integrand is the velocity–velocity autocorrelation function over individual particle trajectories.[45–47] Note that in taking the time integral and assuming time translation invariance, one can recover the conventional random walk formula for the diffusion coefficient in terms of the mean-square displacement $\langle|\mathbf{r}_i|^2\rangle$. In the case of tracer diffusion, the effects of varying composition on the diffusivity are entirely characterized by the prefactors $p_{d,q}$ in (1).

Long-wavelength fluctuations in the particle density, due either to an external perturbation or to local thermal fluctuations, introduce finite concentration gradients into the system. The relaxation of the system back toward equilibrium is then controlled by the collective diffusion of an ensemble of particles, characterized by the chemical diffusion coefficient $D_{\alpha,\mathrm{chem}}$. Again, this transport coefficient can be formally defined in the Green–Kubo linear response formalism,[47,48]

$$D_{\alpha,\mathrm{chem}} = \frac{\Theta_\alpha}{N_\alpha d}\int_0^\infty dt\left\langle\sum_{i=1}^{N_\alpha}\mathbf{v}_i(t)\cdot\sum_{j=1}^{N_\alpha}\mathbf{v}_j(0)\right\rangle, \tag{6}$$

where the velocity–velocity correlation function captures the time correlation of the total flux of particles of species α. This correlation function can be related to the mean-square displacement of the center of mass coordinate of the ensemble of particles, $\left\langle\left|\sum_{i=1}^{N_\alpha}\mathbf{r}_i\right|^2\right\rangle/N_\alpha$. The so-called thermodynamic factor,

$$\Theta_\alpha = \left(\frac{\langle(\delta N_\alpha)^2\rangle}{\langle N_\alpha\rangle}\right)^{-1} = \frac{\partial(\mu_\alpha/k_\mathrm{B}T)}{\partial\ln k_\alpha}, \tag{7}$$

accounts for the chemical non-ideality of the system[49] and amounts to an additional thermodynamic driving force due to the change in chemical potential with changes in composition. Its presence in (6) follows fundamentally from the fluctuation–dissipation theorem under the assumption that local detailed balance is satisfied.[45–48] We further note that this assumption is valid when Fick's law continues to hold,[46] that is, in the linear response regime. In comparing these expressions for tracer (5) and chemical (6) diffusion coefficients, the terms related to cross correlations between distinct pairs ($i \neq j$) of particle trajectories in chemical diffusion typically lead to additional factors of $O(1)$ for self-diffusion.[45,49] We have previously verified that this is the case for vacancy-mediated Cu diffusion using KLMC.[28] Neglecting these cross correlations then leads to the following approximation for chemical diffusion:

$$D_{\alpha,\mathrm{chem}} \approx \Theta_\alpha D_\alpha^*, \tag{8}$$

originally due to Reed and Ehrlich.[50] Thus, D_α^* approximately equals $D_{\alpha,\mathrm{chem}}$ when interactions between diffusing particles can be ignored ($\Theta_\alpha = 1$), applicable, for instance, to the case of radioactive tracers in the dilute limit.

For materials such as CIS that can exhibit large deviations from ideal stoichiometry, we will find below (Sec. III A) that the thermodynamic factor can provide a significant correction to tracer diffusion in the presence of finite concentration gradients. In modeling the dependence of the chemical potentials on the chemical compositions in the CCT formalism, we can compute thermodynamic factors by simply evaluating numerical gradients (7) at every point in the equilibrium phase diagram. In doing so, the derived thermodynamic factors account for the highly nontrivial relationship between the formation of intrinsic defects in CIS and its thermodynamic stability. It is again worth emphasizing that this is fundamentally a linear response approximation. Therefore, a direct calculation of $D_{\alpha,\mathrm{chem}}$ based on equilibrium ensemble averages assumes that the macroscopic perturbations to the composition that drive collective diffusion are not far away from the reference equilibrium state. In other words, equilibrium is assumed to set in locally over intermediate space and time scales, which are greater than the particles' mean free path and equilibrium relaxation time but less than the typical experimental resolution for measuring depth profiles. To assess the validity of this approximation and the consistency of the underlying atomistic picture presented in Sec. III A, we consider a particularly nonequilibrium situation involving the inward diffusion of Cu in CIS from a Cu-rich boundary source,[22] which we then simulate using a minimal reaction–diffusion model in Sec. III B.

30 August 2023 13:45:23

Published under an exclusive license by AIP Publishing

III. RESULTS AND DISCUSSION

We have considered the following diffusion pathways:

$$V_{Cu} \rightarrow V_{Cu}, \tag{9}$$

$$Cu_i \rightarrow Cu_i, \tag{10}$$

$$Cu_{In} + V_{In} \rightarrow V_{In} + Cu_{In}, \tag{11}$$

$$Cu_i \rightarrow (Cu - Cu)_{Cu} \rightarrow Cu_i. \tag{12}$$

Based on Eq. (1) and CCT calculations, we have determined that Cu diffuses primarily via exchange with Cu vacancies (9) and via interstitial sites (10). Cu_{In} antisite diffusion via In vacancies (11) can be safely excluded from our model because the probability $(x_{Cu_{In}} x_{V_{In}})/(k_{Cu} k_{In})$ is irrelevant compared to (9) and (10) over the compositions considered, and local binding between the defects is unfavorable due to repulsive Coulomb interactions. For simplicity, we have also excluded the indirect interstitialcy diffusion pathway (12). Since this pathway has been found to have a migration barrier similar to direct interstitial diffusion,[27,51] it can be effectively incorporated into our model for direct interstitial diffusion by modifying the local coordination number, z, and the correlation factor,[49] f. This amounts to a correction to the diffusivity by a factor of $O(1)$.

Values for the parameters in Eq. (1) for V_{Cu}-mediated and direct interstitial diffusion are listed in Table I. Since V_{Cu} acts as a shallow acceptor, both the neutral and (1−) charge states occur in significant quantities in p-type, Cu-poor material and are furthermore found to have similar migration barriers. Both charge states are, therefore, included in the vacancy model. We previously found[28] that V_{Cu} hops between second nearest-neighbor sites (2NN) on the Cu sublattice possess migration barriers comparable with those of the conventional 1NN processes. Hence, these 2NN processes are also considered. However, it is worth noting that the small anisotropy between c and a, b lattice vectors in the conventional chalcopyrite unit cell of CIS reduces the effective dimensionality of the 2NN processes [Fig. 2(b)]. While the local 1NN sublattice environment is tetrahedrally coordinated, similar to a zinc-blend lattice, the relative 2NN connectivity is not, likewise, face-center cubic. Alternatively, 2NN sites are connected in parallel 2D square lattices, which form planes normal to the c axis, and hence, strict diffusion via 2NN hopping is quasi-two-dimensional. The correlation factors shown in Table I reflect this local connectivity.[30] Since Cu interstitials act as shallow donors and the prevalence of Cu vacancies limits the degree of n-type self-doping in CIS,[52] we only consider Cu_i in the (1+) charge state.

TABLE I. Parameters (1) for vacancy- and interstitial-mediated Cu diffusion in net charge state q.

Mechanism	$p_{i,q}$	λ	z (d)	f	ν	$\Delta E_{i,q}^{(m)}$ (q)
V_{Cu} (1NN)	$\frac{x_{V_{Cu},q}}{k_{Cu}}$	4.17	4 (3)	0.50	18.8	1.10 (0), 1.12 (1 −)
V_{Cu} (2NN)	$\frac{x_{V_{Cu},q}}{k_{Cu}}$	5.88	4 (2)	0.47	34.7	1.20 (0), 1.21 (1 −)
Cu_i	$\frac{x_{Cu_i,q}}{k_{Cu}}$	4.18	12 (3)	1.0	1.1	0.26 (1+)

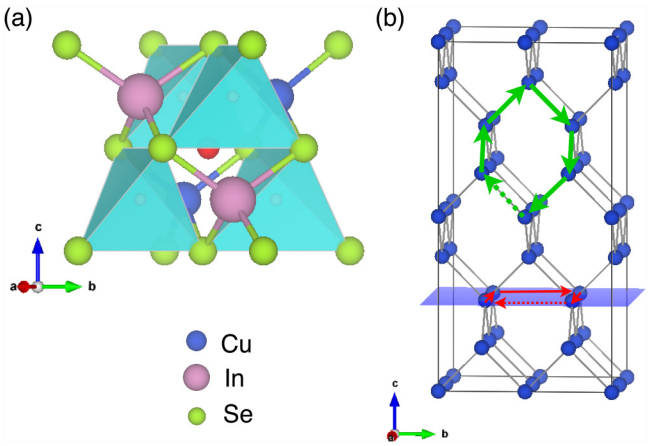

FIG. 2. (a) Local arrangement of lowest-energy Cu interstitial sites in chalcopyrite CIS (center of blue tetrahedra). Direct Cu interstitial diffusion proceeds by local hopping through the saddle point (red sphere). (b) 1NN (green arrows) and 2NN (red arrows) hops associated with vacancy-mediated diffusion on the Cu sublattice. Closed paths show the minimum number of hops leading to net displacement of a Cu tracer, leading to correlation factors below unity.[30,49] Note that strictly 2NN vacancy diffusion is restricted to the *ab* planes (blue) normal to the *c* axis.

A. Cu tracer and chemical self-diffusion

Figures 3(b) and 3(c) exhibit the variation in the chemical and tracer Cu diffusivities across the stable thermodynamic range of CIS. The data are shown at 700 K, chosen to be within the range of both typical synthesis temperatures and reported temperatures for experimental Cu diffusion measurements.[20,22,23,53] We find that the tracer diffusion coefficient ranges over several orders of magnitude, 10^{-12}–10^{-7} cm^2/s, where the largest values occur for sufficiently Cu-poor and Cu-rich compositions, separated by a local minimum that spans the range of Se chemical potentials. This composition dependence is shown in Fig. 3(a) corresponding to a cut across the phase diagram with fixed Se chemical potential, chosen to reflect typical synthesis conditions for p-type material with fixed Se partial pressure. We also show the individual contributions from vacancy- and interstitial-mediated mechanisms to the total diffusivity. As expected, the vacancy mechanisms dominate the diffusion in Cu-poor material, the interstitial mechanism becomes dominant for Cu-rich material, and the crossover between the two regimes results in the local minimum in the total diffusivity. We find that the value at this local minimum agrees with the value measured by Gartsman *et al.*[22] for the bulk diffusion of dilute Cu tracers. Furthermore, we find that maximal tracer diffusivities can be achieved either at the Cu_2Se-pure Cu secondary phase boundaries or for sufficiently excess Se chemical potential.

The chemical diffusion coefficient, on the other hand, takes on typical values on the order of 10^{-9}–10^{-8} cm^2/s throughout most

30 August 2023 13:45:23

Published under an exclusive license by AIP Publishing

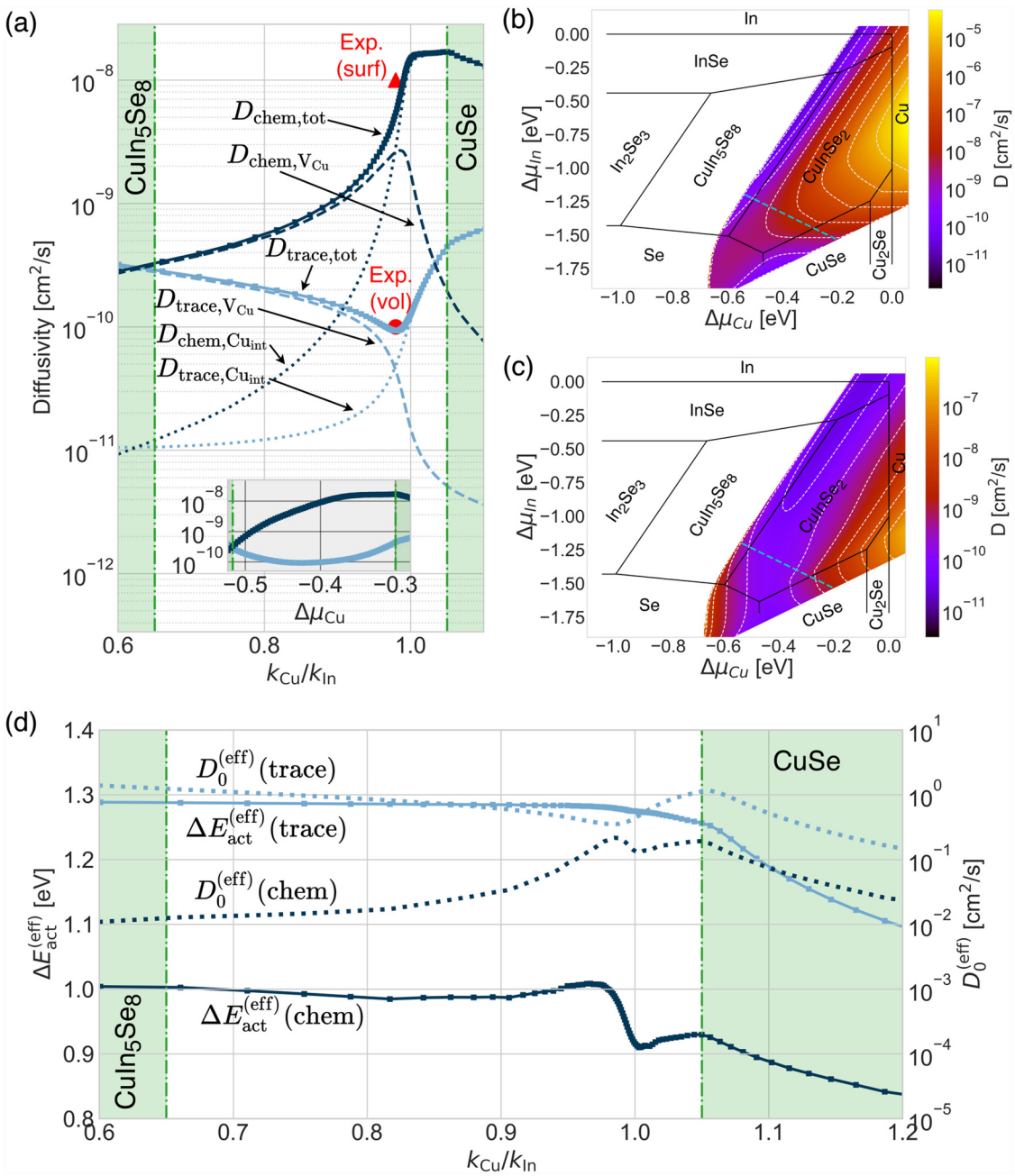

FIG. 3. (a) Dependence of the Cu tracer and chemical diffusion coefficients on the [Cu]/[In] ratio for fixed Se chemical potential at 700 K. The Se chemical potential is chosen to reflect excess Se supply during material synthesis. The diffusivities in (a) are plotted along the cut (blue, dashed line) through the phase diagram, shown in (b) and (c), and the corresponding locations of the predicted secondary phase boundaries are shown in green. The individual contributions from vacancy- and interstitial-mediated mechanisms to the total diffusivity are shown for both tracer and chemical diffusion. The red data points labeled "Exp. (vol)" and "Exp. (surf)" are the measured diffusivities reported by Gartsman *et al.*[22] for radiotracer volume diffusion and inward Cu diffusion following CIS surface deposition of a Cu film, respectively. The [Cu]/[In] positions for these points were determined by the reported stoichiometries of their single crystal CIS samples.[22] The inset to (a) shows the Cu chemical potential dependence of the total tracer and chemical diffusion coefficients along the same cut in (b) and (c). The full dependence of the chemical (b) and tracer (c) diffusion coefficients on the Cu and In chemical potentials in stable CIS is also shown. Sparse isocurves (white, dashed curves) are included to highlight the nonlinearity of the two diffusivities in the chemical potential space. (d) Effective activation energies and diffusivity prefactors from Arrhenius fits (13) to the temperature dependence of the chemical and tracer diffusion coefficients. The composition dependence is taken along the same cut in the phase diagram (b) and (c) with constant Se chemical potential.

30 August 2023 13:45:23

Published under an exclusive license by AIP Publishing

of the stable CIS region. The diffusivity reaches its lowest values along the Cu-depleted phase boundary and near the intersection with the Se and CuSe boundaries. The higher chemical diffusion coefficients obtained in the bulk of the stable CIS region are due to the relatively large changes in chemical potential required to move the material to either Cu-rich or Cu-poor off-stoichiometries. Hence, in the presence of perturbations to the equilibrium Cu compositions, there is a strong thermodynamic driving force back toward equilibrium. For Cu-rich material with an appreciably higher concentration of rapidly diffusing interstitials, this leads to a significantly larger chemical diffusion coefficient. This agrees with the findings of Gartsman *et al.*,[22] for the inward diffusion of Cu following the surface deposition of a Cu film. In this case, we find that the total chemical diffusion within the CIS layer is controlled by local fluctuations in the Cu composition [Fig. 3(a)], and moreover that both interstitial- and vacancy-mediated mechanisms are important. We can rationalize this situation by considering the following microscopic picture. Cu deposited on the surface of moderately Cu-poor, Se-rich CIS yields a Cu-rich interface region that favors the formation of Cu interstitials.[39] The low migration barriers of these interstitials enable their rapid diffusion into the bulk CIS. Far away from this interface region, CIS remains Cu-poor, and the associated high number of Cu vacancies eventually limits the inward diffusion of interstitials via Frenkel pair recombination. In Sec. III B, we validate the fundamental kinetics in this picture by constructing and simulating an approximate continuum model.

The temperature dependence of the total tracer and chemical diffusivities can be approximated by an Arrhenius function,

$$D_{\mathrm{tot}}(T) = D_0^{(\mathrm{eff})} e^{-\Delta E_{\mathrm{act}}^{(\mathrm{eff})}/k_{\mathrm{B}}T}, \tag{13}$$

where the effective activation energy, $\Delta E_{\mathrm{act}}^{(\mathrm{eff})}$, and diffusion prefactor, $D_0^{(\mathrm{eff})}$, are determined by fits to our numerical data. Figure 3(d) shows the cation ratio dependence of these effective parameters along the same constant Se chemical potential contour considered previously. The effective activation energy for tracer diffusion is within the range of values, 1.25 ± 0.10 eV, reported by Becker and Wagner[20] across the chemical compositions considered. However, it is important to note that while this activation energy is closer to the vacancy-mediated migration barriers, a vacancy mechanism does not completely explain the result. Indeed, as discussed above, diffusion is dominated in Cu-rich CIS by an interstitial mechanism. The crossover between vacancy- and interstitial-dominated regimes is apparent in the onset of nonlinearity in the effective activation energies and prefactors as $k_{\mathrm{Cu}}/k_{\mathrm{In}} \to 1$. As expected, the inclusion of a thermodynamic factor yields Arrhenius fits to the chemical diffusion coefficient that result in effective activation energies lower than their tracer counterparts. This agrees, at least qualitatively, with the lower experimental activation energies, ≈0.55–0.75 eV, reported in Refs. 29 and 54 for chemical diffusion, although it appears that these values were based on averaging across samples with different compositions. Nonetheless, for tracer and chemical diffusion, we find that the effective activation energies are lowered as the material becomes increasingly Cu-rich, signaling faster diffusion with the introduction of more Cu interstitials.

B. Inward diffusion from a Cu-rich boundary

To directly study the influence of a nonequilibrium distribution of Cu defects on Cu diffusion, we simulated the in-diffusion of Cu tracers from a layer of Cu deposited on the CIS surface and compared the predicted depth profiles to those reported by Gartsman *et al.*[22] To that end, we define a simple, continuum reaction–diffusion model for Cu consisting of vacancy- and interstitial-mediated diffusion and Frenkel pair recombination/generation,

$$\partial_t C_{\mathrm{V_{Cu}}} = \left(D_{\mathrm{V_{Cu}}}^{(1)} + D_{\mathrm{V_{Cu}}}^{(2)}\right)\nabla^2 C_{\mathrm{V_{Cu}}} - R_{\mathrm{F}} - R_{\mathrm{F}^\dagger}, \tag{14}$$

$$\partial_t C_{\mathrm{Cu}_i} = D_{\mathrm{Cu}_i}\nabla^2 C_{\mathrm{Cu}_i} - R_{\mathrm{F}}, \tag{15}$$

$$\begin{aligned} \partial_t C_{\mathrm{Cu}_i^\dagger} &= D_{\mathrm{Cu}_i}\nabla^2 C_{\mathrm{Cu}_i^\dagger} - R_{\mathrm{F}^\dagger}, \\ \partial_t C_{\mathrm{Cu}_{\mathrm{Cu}}^\dagger} &= \left(f^{(1)} D_{\mathrm{V_{Cu}}}^{(1)} + f^{(2)} D_{\mathrm{V_{Cu}}}^{(2)}\right)\frac{C_{\mathrm{V_{Cu}}}}{C_{\mathrm{s}}} \end{aligned} \tag{16}$$

$$\times \nabla^2 C_{\mathrm{Cu}_{\mathrm{Cu}}^\dagger} + R_{\mathrm{F}^\dagger}, \tag{17}$$

where a "†" on a chemical component denotes a tracer species, C_i is the per volume concentration of vacancies, interstitials or lattice Cu, and C_{s} is the concentration of Cu sublattice sites. The superscripts (1) and (2) refer to the 1NN and 2NN vacancy-mediated diffusion mechanisms, where $f^{(1)}$ and $f^{(2)}$ are the respective correlation factors. Since the barriers for 1NN and 2NN vacancy-mediated diffusion are nearly equal (see Table I), we treat these coefficients as independent from the charge state of the vacancy. The Frenkel pair reaction rates R_{F} and $R_{\mathrm{F}^\dagger}$ are defined for non-tracers and tracers, respectively, as

$$R_{\mathrm{F}} = k_f\left(C_{\mathrm{V_{Cu}}}C_{\mathrm{Cu}_i} - C^*_{\mathrm{V_{Cu}}}C^*_{\mathrm{Cu}_i}\right), \tag{18}$$

$$R_{\mathrm{F}^\dagger} = k_f\left(C_{\mathrm{V_{Cu}}}C_{\mathrm{Cu}_i^\dagger} - C_{\mathrm{Cu}_{\mathrm{Cu}}^\dagger}\frac{C^*_{\mathrm{V_{Cu}}}C^*_{\mathrm{Cu}_i}}{C^*_{\mathrm{Cu_{Cu}}}}\right), \tag{19}$$

$$k_f = 4\pi\lambda_{IV}\left(D_{\mathrm{V_{Cu}}}^{(1)} + D_{\mathrm{V_{Cu}}}^{(2)} + D_{\mathrm{Cu}_i}\right). \tag{20}$$

Since the energy barrier for Frenkel pair recombination ($\mathrm{V_{Cu}} + \mathrm{Cu}_i \to \mathrm{Cu_{Cu}}$) is low relative to the migration barriers, $\Delta E_{IV} = 0.13$ eV, the forward-reaction rate, k_f, is diffusion-limited. The capture cross section for Frenkel pair recombination is determined by the nearest-neighbor distance ($\lambda_{IV} \approx 2.95$ Å) between interstitial and Cu-sublattice sites. Bulk equilibrium concentrations, C^*, were determined by CCT calculations using compositions within the range reported by Gartsman *et al.*[22] The simulations were carried out using the finite-element solvers in Synopsys's Sentaurus Process.

To model the presence of Cu at the CIS surface, we imposed simple Dirichlet boundary conditions, where surface defect equilibrium concentrations were determined by selecting the material composition at which the corresponding chemical potentials were

30 August 2023 13:45:23

Published under an exclusive license by AIP Publishing

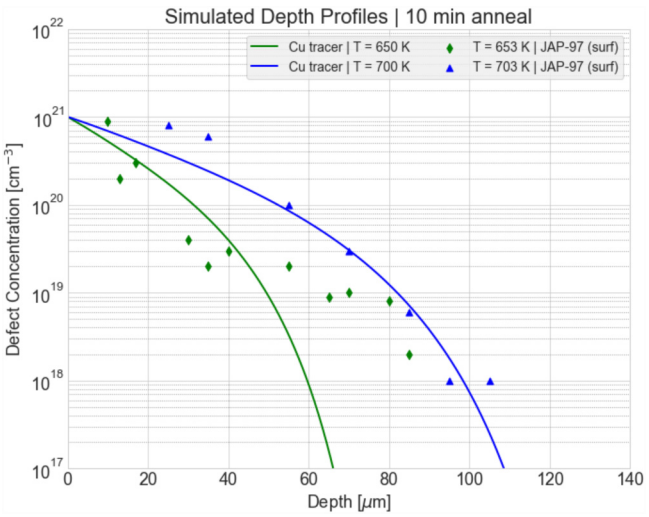

FIG. 4. Simulated depth profiles for the in-diffusion of Cu tracers from a surface layer of Cu into Cu-poor, *p*-type CIS compared to experimental values reported in JAP-97.[22]

in equilibrium with face-center cubic Cu and secondary phase Cu_2Se. The surface concentration of lattice Cu tracers is a free parameter in our model, which we set according to the initial dose estimated from the depth profiles reported by Gartsman *et al.*[22] We note that, in formulating this reaction–diffusion model (17), we have assumed that the depletion of Cu tracers at the boundary is negligible on the relevant time scales we wish to simulate, which is consistent with the large reported dose of surface Cu.[22]

Figure 4 shows the simulated diffusion profiles for the in-flow of Cu tracers under a 10 min anneal at 650 and 700 K. We find excellent agreement between our model and the reported data at 703 K, while our model does not account for the long tail observed experimentally at 653 K. Nonetheless, we find that the rapid in-diffusion of Cu, with a diffusivity two orders of magnitude greater than the reported bulk diffusivity, can be accounted for by the injection of Cu interstitials from secondary Cu-rich phases at the CIS surface.

IV. SUMMARY

Gartsman *et al.*[22] and Lubomirsky *et al.*[29] found a consistent two orders of magnitude difference between the diffusion of Cu measured by tracking bulk Cu tracers vs measurements based on Cu in-diffusion and *p–n* junction motion. Absent space charge effects, they attributed this difference to the presence of a large thermodynamic factor on the order of $\Theta \approx 100$. The results presented in this work support this argument. Indeed, by employing a model of intrinsic defect thermodynamics in CIS coupled via compositional constraints, we have directly calculated thermodynamic factors of this magnitude in a moderately Cu-poor, Se-rich *p*-type material and explored their impact on the predicted diffusion coefficients. Our predictions for both tracer and chemical coefficients were shown to be in close agreement with the experimental measurements reported by Gartsman *et al.*,[22] and this further validates the outsized effects that thermodynamic driving forces can have on chemical diffusion in heavily compensated materials such as CIS. Moreover, we have related this linear response picture to the underlying correlated random walks executed by individual Cu atoms, hopping either through vacant Cu-sublattice sites or through interstitial pathways. A relatively simple continuum model based on this atomistic picture was able to approximately reproduce the experimental diffusion profiles[22] for the in-flow of Cu into Cu-poor CIS from a Cu-rich interface, demonstrating how Cu interstitials, in particular, can lead to enhanced Cu diffusion. Finally, by mapping out the behavior of the tracer and chemical diffusion coefficients across the CIS secondary phase diagram, we have predicted the extent to which either variations in the composition or the material synthesis conditions can account for the large spread of reported Cu diffusivities measured at elevated temperatures.

ACKNOWLEDGMENTS

This material is based upon work supported by the Department of Energy (DOE) under Award No. DE-EE0008556. This work was facilitated through the use of an advanced computational, storage, and networking infrastructure provided by the Hyak supercomputer system at the University of Washington, funded by the UW Student Technology Fee.

AUTHOR DECLARATIONS

Conflict of Interest

The authors have no conflicts to disclose.

DATA AVAILABILITY

The data that support the findings of this study are available from the corresponding author upon reasonable request.

APPENDIX: DETAILS FOR FIRST-PRINCIPLES CALCULATIONS

All first-principles calculations in this work were carried out using the Vienna *Ab Initio* Simulation Package (VASP).[35,55] Plane-wave, Kohn–Sham density functional theory calculations employed the all-electron projector-augmented wave (PAW) method.[56,57] Due to the large number of calculations required to build a set of reference formation energies and the computational demand of *ab initio* methods, we use the efficient Perdew–Burke–Ernzerhof (PBE)[58] generalized gradient approximation (GGA) functional rather than a potentially more accurate, but much more computationally intensive, method such as hybrid Heyd–Scuseria–Ernzerhof (HSE).[59] HSE provides an improved description of the localized 3*d*-orbitals of Cu-containing semiconductor compounds compared to local density functionals.[9,36] We approximated this behavior to correct for the underestimated bandgap predicted by GGA by applying a +U correction (U = +5 eV) to the Cu *d* states following the method of Dudarev *et al.*[60] Ground state energy calculations were performed using a 64-atom cell and a $2 \times 2 \times 2$ Monkhorst–Pack k-point mesh,[61] and the intra-ionic Hellmann–Feynman forces

30 August 2023 13:45:23

Published under an exclusive license by AIP Publishing

were relaxed to below 0.01 eV/Å. For defect formation energies and charge transition levels, we included post-processing corrections for spurious electrostatic interactions following the scheme (FNV) proposed by Freysoldt, Neugebauer, and Van de Walle.[62] Migration energy barriers were calculated using the climbing-image nudged elastic band (CINEB) method,[34] while normal vibrational modes were calculated using density functional perturbation theory (DFPT). Visualizations of atomic structures (Fig. 2) were generated using the VESTA program.[63]

REFERENCES

[1]P. Jackson, D. Hariskos, E. Lotter, S. Paetel, R. Wuerz, R. Menner, W. Wischmann, and M. Powalla, Prog. Photovolt. Res. Appl. **19**, 894 (2011).
[2]R. Scheer and H.-W. Schock, *Chalcogenide Photovoltaics: Physics, Technologies, and Thin Film Devices* (John Wiley & Sons, 2011).
[3]P. Reinhard, A. Chirilă, P. Blösch, F. Pianezzi, S. Nishiwaki, S. Buecheler, and A. N. Tiwari, in *2012 IEEE 38th Photovoltaic Specialists Conference (PVSC) PART 2* (IEEE, 2012), pp. 1–9.
[4]A. Chirilă, P. Reinhard, F. Pianezzi, P. Bloesch, A. R. Uhl, C. Fella, L. Kranz, D. Keller, C. Gretener, H. Hagendorfer *et al.*, Nat. Mater. **12**, 1107 (2013).
[5]P. Jackson, D. Hariskos, R. Wuerz, O. Kiowski, A. Bauer, T. M. Friedlmeier, and M. Powalla, Phys. Status Solidi RRL. **9**, 28 (2015).
[6]P. Jackson, R. Wuerz, D. Hariskos, E. Lotter, W. Witte, and M. Powalla, Phys. Status Solidi RRL. **10**, 583 (2016).
[7]C. Spindler, F. Babbe, M. H. Wolter, F. Ehré, K. Santhosh, P. Hilgert, F. Werner, and S. Siebentritt, Phys. Rev. Mater. **3**, 090302 (2019).
[8]S. B. Zhang, S. H. Wei, A. Zunger, and H. Katayama-Yoshida, Phys. Rev. B **57**, 9642 (1998).
[9]J. Pohl and K. Albe, Phys. Rev. B **87**, 245203 (2013).
[10]B. Tell, J. Shay, and H. Kasper, J. Appl. Phys. **43**, 2469 (1972).
[11]P. Migliorato, J. Shay, H. Kasper, and S. Wagner, J. Appl. Phys. **46**, 1777 (1975).
[12]R. Noufi, R. Axton, C. Herrington, and S. Deb, Appl. Phys. Lett. **45**, 668 (1984).
[13]M. L. Fearheiley, Solar Cells **16**, 91 (1986).
[14]S. Siebentritt, L. Gütay, D. Regesch, Y. Aida, and V. Deprédurand, Sol. Energy Mater. Sol. Cells **119**, 18 (2013).
[15]D. Colombara, K. Conley, M. Malitckaya, H.-P. Komsa, and M. J. Puska, J. Mater. Chem. A **8**, 6471 (2020).
[16]D. Colombara, F. Werner, T. Schwarz, I. C. Infante, Y. Fleming, N. Valle, C. Spindler, E. Vacchieri, G. Rey, M. Guennou *et al.*, Nat. Commun. **9**, 826 (2018).
[17]J. F. Guillemoles, L. Kronik, D. Cahen, and U. Rau, J. Phys. Chem. B **104**, 4849 (2000).
[18]T. Nishimura, S. Toki, H. Sugiura, K. Nakada, and A. Yamada, Appl. Phys. Express **9**, 092301 (2016).
[19]S. Ji, T. Hayakawa, N. Suyama, K. Nakada, and A. Yamada, Jpn. J. Appl. Phys. **59**, 041003 (2020).
[20]K. D. Becker and S. Wagner, Phys. Rev. B **27**, 5240 (1983).
[21]G. Dagan, T. F. Ciszek, and D. Cahen, J. Phys. Chem. **96**, 11009 (1992).
[22]K. Gartsman, L. Chernyak, V. Lyahovitskaya, D. Cahen, V. Didik, V. Kozlovsky, R. Malkovich, E. Skoryatina, and V. Usacheva, J. Appl. Phys. **82**, 4282 (1997).
[23]I. Lyubomirsky, M. K. Rabinal, and D. Cahen, J. Appl. Phys. **81**, 6684 (1997).
[24]P. E. Stallworth, J.-F. Guillemoles, J. Flowers, J. Vedel, and S. G. Greenbaum, Solid State Commun. **113**, 527 (2000).
[25]D. Soltz, G. Dagan, and D. Cahen, Solid State Ion. **28**, 1105 (1988).
[26]J. Pohl and K. Albe, J. Appl. Phys. **108**, 023509 (2010).
[27]J. Pohl, A. Klein, and K. Albe, Phys. Rev. B **84**, 121201 (2011).
[28]D. E. Sommer and S. T. Dunham, J. Appl. Phys. **123**, 115116 (2018).
[29]I. Lubomirsky, K. Gartsman, and D. Cahen, J. Appl. Phys. **83**, 4678 (1998).
[30]H. Mehrer, *Diffusion in Solids: Fundamentals, Methods, Materials, Diffusion-Controlled Processes*, Springer Series in Solid-State Sciences Vol. 155 (Springer, 2007).
[31]D. E. Sommer, D. Mutter, and S. T. Dunham, IEEE J. Photovolt. **7**, 1143 (2017).
[32]G. H. Vineyard, J. Phys. Chem. Solids **3**, 121 (1957).
[33]M. Mantina, Y. Wang, R. Arroyave, L. Q. Chen, Z. K. Liu, and C. Wolverton, Phys. Rev. Lett. **100**, 215901 (2008).
[34]G. Henkelman and B. P. Uberuaga, J. Chem. Phys. **113**, 9901 (2000).
[35]G. Kresse and J. Furthmüller, Phys. Rev. B **54**, 11169 (1996).
[36]C. Freysoldt, B. Grabowski, T. Hickel, and J. Neugebauer, Rev. Mod. Phys. **86**, 253 (2014).
[37]D. Mutter and S. T. Dunham, IEEE J. Photovolt. **5**, 1188 (2015).
[38]T. Gödecke, T. Haalboom, and F. Ernst, Z. Metallkd. **91**, 622 (2000).
[39]R. Herberholz, U. Rau, H. W. Schock, T. Haalboom, T. Gödecke, F. Ernst, C. Beilharz, K. W. Benz, and D. Cahen, Eur. Phys. J. Appl. Phys. **6**, 131 (1999).
[40]S. Zhang, S.-H. Wei, A. Zunger, and H. Katayama-Yoshida, Phys. Rev. B **57**, 9642 (1998).
[41]C. D. Ludwig, T. Gruhn, C. Felser, and J. Windeln, Phys. Rev. B **83**, 174112 (2011).
[42]J. Bekaert, R. Saniz, and B. Partoens, Phys. Chem. Chem. Phys. **16**, 22299 (2014).
[43]F. Werner, D. Colombara, M. Melchiorre, N. Valle, B. E. Adib, C. Spindler, and S. Siebentritt, J. Appl. Phys. **119**, 173103 (2016).
[44]D. Colombara, H. Elanzeery, N. Nicoara, D. Sharma, M. Claro, T. Schwarz, A. Koprek, M. H. Wolter, M. Melchiorre, M. Sood *et al.*, Nat. Commun. **11**, 3634 (2020).
[45]R. Gomer, Rep. Prog. Phys. **53**, 917 (1990).
[46]T. Ala-Nissila, R. Ferrando, and S. Ying, Adv. Phys. **51**, 949 (2002).
[47]G. F. Mazenko, in *Surface Mobilities on Solid Materials* (Springer, 1983), pp. 27–62.
[48]D. Forster, *Hydrodynamic Fluctuations, Broken Symmetry, and Correlation Functions*, Frontiers in Physics (Benjamin/Cummings, 1975).
[49]A. R. Allnatt and A. B. Lidiard, *Atomic Transport in Solids* (Cambridge University Press, 1993).
[50]D. A. Reed and G. Ehrlich, Surf. Sci. **102**, 588 (1981).
[51]L. E. Oikkonen, M. G. Ganchenkova, A. P. Seitsonen, and R. M. Nieminen, J. Phys.: Condens. Matter **26**, 345501 (2014).
[52]C. Persson, Y. J. Zhao, S. Lany, and A. Zunger, Phys. Rev. B **72**, 035211 (2005).
[53]B. Tell and P. M. Bridenbaugh, J. Appl. Phys. **48**, 2477 (1977).
[54]L. Chernyak, K. Gartsman, D. Cahen, and O. M. Stafsudd, J. Phys. Chem. Solids **56**, 1165 (1995).
[55]G. Kresse and J. Furthmüller, Comput. Mater. Sci. **6**, 15 (1996).
[56]W. Kohn and L. J. Sham, Phys. Rev. **140**, A1133 (1965).
[57]P. E. Blöchl, Phys. Rev. B **50**, 17953 (1994).
[58]J. P. Perdew, K. Burke, and M. Ernzerhof, Phys. Rev. Lett. **77**, 3865 (1996).
[59]J. Heyd, G. E. Scuseria, and M. Ernzerhof, J. Chem. Phys. **118**, 8207 (2003).
[60]S. Dudarev, G. Botton, S. Savrasov, C. Humphreys, and A. Sutton, Phys. Rev. B **57**, 1505 (1998).
[61]H. Monkhorst and J. Pack, Phys. Rev. B **13**, 5188 (1976).
[62]C. Freysoldt, J. Neugebauer, and C. G. Van de Walle, Phys. Rev. Lett. **102**, 016402 (2009).
[63]K. Momma and F. Izumi, J. Appl. Crystallogr. **44**, 1272 (2011).

30 August 2023 13:45:23

Published under an exclusive license by AIP Publishing